

# Femtosecond Soft X-ray Absorption Spectroscopy Identifies Metal-Centered $S_1$ Excited State of Cyanocobalamin

Nahid Ghodrati,<sup>†</sup> Luigi Adriano,<sup>†</sup> Samuel M. Berry,<sup>‡</sup> Camille Carinan,<sup>†</sup> Robert Carley,<sup>†</sup> Yi-Ping Chang,<sup>†</sup> Cyril Danilevski,<sup>†</sup> Christian David,<sup>¶</sup> Robin Engel,<sup>§</sup> Natalia Gerasimova,<sup>†</sup> David Hammer,<sup>†</sup> Manuel Harder,<sup>†</sup> Ryan M. Lamb,<sup>‡</sup> David Lomidze,<sup>†</sup> Talgat Mamyrbayev,<sup>¶</sup> Matteo Porro,<sup>†, #</sup> Martin Teichmann,<sup>†</sup> Monica Turcato,<sup>†</sup> Joana Valerio,<sup>†</sup> Ru-Pan Wang,<sup>||</sup> Zhong Yin,<sup>⊥</sup> Andreas Scherz,<sup>†</sup> Nils Huse,<sup>||, @</sup> James E. Penner-Hahn,<sup>‡, Δ</sup> Roseanne J. Sension,<sup>‡, ∇</sup> Loïc Le Guyader,<sup>\*, †</sup> and Benjamin E. Van Kuiken<sup>\*, †</sup>

<sup>†</sup>*European XFEL, Holzkoppel 4, 22869 Schenefeld, Germany*

<sup>‡</sup>*Department of Chemistry, University of Michigan, 930 N University Avenue, Ann Arbor, Michigan 48109-1055, United States*

<sup>¶</sup>*Paul Scherrer Institute, 5232 Villigen PSI, Switzerland*

<sup>§</sup>*Deutsches Elektronen-Synchrotron DESY, Notkestr. 85, 22607, Hamburg, Germany*

<sup>||</sup>*Institute for Nanostructure and Solid State Physics, University of Hamburg, Luruper Chaussee 149, 22761 Hamburg*

<sup>⊥</sup>*International Center for Synchrotron Radiation Innovation Smart, Tohoku University, 980-8577 Sendai, Japan*

<sup>#</sup>*Department of Molecular Sciences and Nanosystems, Ca Foscari University of Venice, 30172 Venice, Italy*

<sup>@</sup>*Center for Free Electron Laser Science, Luruper Chaussee 149, 22761 Hamburg, Germany*

<sup>Δ</sup>*Department of Biophysics, University of Michigan, 930 N University Avenue, Ann Arbor, Michigan 48109-1055, United States*

<sup>∇</sup>*Department of Physics, University of Michigan, 450 Church Street, Ann Arbor, Michigan 48109-1040, United States*

E-mail: loic.le.guyader@xfel.eu; benjamin.van.kuiken@xfel.eu

**Abstract**

Time-resolved X-ray absorption spectroscopy (TRXAS) at the Co L<sub>3</sub>-edge was used to identify metal-centered (MC) character in the S<sub>1</sub> excited state of cyanocobalamin (CNCbl). Cobalamins have UV/visible spectra that are dominated by intense corrin-based excitations, but these ligand-centered states energetically overlap with charge transfer and MC excited states that may be populated following photoexcitation. Ultrafast optical and hard X-ray spectroscopy have shown that CNCbl forms a structurally distorted S<sub>1</sub> state, but these probes lack a clear signature of the S<sub>1</sub> electronic identity, which theory has suggested is a ligand-to-metal charge transfer (LMCT) state. Femtosecond soft X-ray TRXAS offers greater state-selectivity than many optical or hard X-ray probes, but has, so far, been limited to highly concentrated ( $\geq 100$  mM) samples. A new experimental setup at the European X-ray Free Electron Laser (EuXFEL) that enables studies of sub-10 mM samples and provides  $\sim 100$  fs time-resolution is used to measure the TRXAS of CNCbl at the Co L<sub>3</sub>-edge. Comparison of the L<sub>3</sub>-edge XAS spectrum measured at 0.8 ps with ligand field multiplet simulations indicates that the S<sub>1</sub> state is primarily a MC excited state. The sub-20  $\mu$ OD detection sensitivity achieved in this study demonstrates the possibility of applying this method to a wide range of naturally-occurring and synthetic transition metal complexes.

## Introduction

Over the last two decades, time-resolved X-ray absorption spectroscopy (TRXAS) employing hard X-rays has become a well-developed technique that permits the study of the ultrafast structural dynamics of transition metal complexes in solution.<sup>1,2</sup> Experiments may be carried out at synchrotrons and X-ray free electron lasers (XFELs), which typically provide  $\sim 100$  ps and  $\sim 100$  fs time resolution, respectively. Measurements are now routinely possible on samples containing transition metal atoms with concentrations of only a few mM such as metalloenzymes and synthetic complexes with low solubility or availability.<sup>3-9</sup> While hard X-ray TRXAS provides transient electronic structure information such as oxidation state

changes, it can be difficult to disentangle the electronic and structural components. Soft X-rays (100 - 1000 eV) offer the possibility of a more direct probe of the electronic structure and higher energy resolution. This range contains the  $L_{2/3}$ -edges ( $2p \rightarrow 3d$ ) providing dipole-allowed transitions to the 3d orbitals for the first row of transition metal elements as well as the K-edges of ligand atoms (C, O, N). Metal L-edge spectroscopy can provide clear signatures of spin, oxidation state, and the chemical bonding environment around the metal.<sup>10-13</sup> The ligand K-edge can report on metal-ligand covalency.<sup>14</sup> Despite the potential of these soft X-ray probes, the adoption of soft X-ray TRXAS as a standard tool to investigate the photochemistry of coordination complexes has been hampered by technical hurdles.

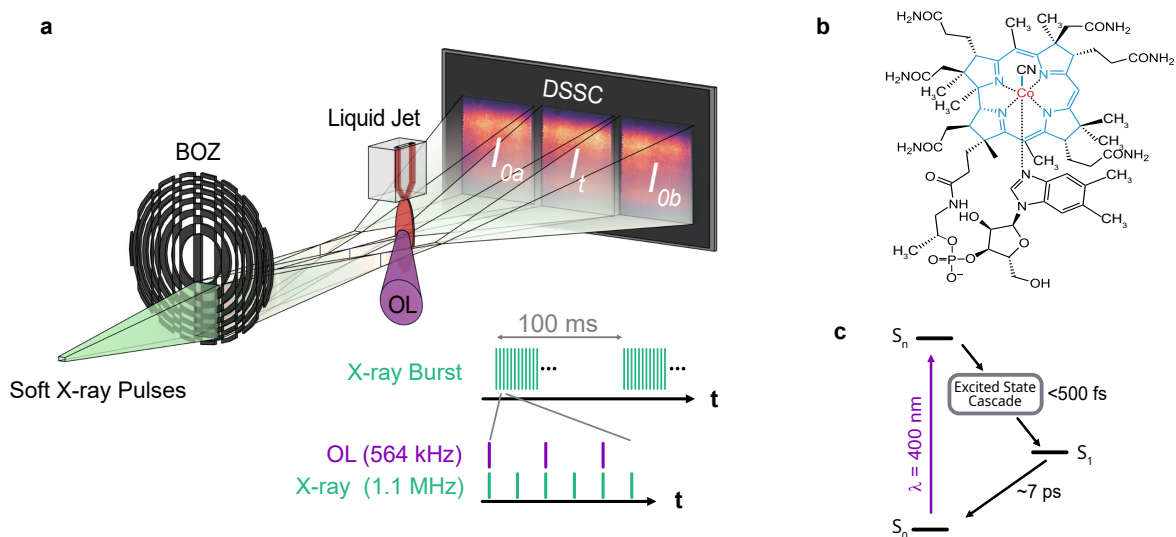


Figure 1: Experimental overview. (a) The BOZ-XAS experimental setup for TRXAS measurements on liquid samples. Monochromatic soft X-rays are delivered by EuXFEL. A beam-splitting off-axis zone plate (BOZ) splits the incident X-ray beam into three copies. The central beam passes through the jet providing a measure of transmitted intensity ( $I_t$ ). The side beams act as reference measurements ( $I_{0a}$  and  $I_{0b}$ ). The DSSC detector performs shot-to-shot detection. The scheme in the bottom right shows the burst mode pulse pattern of the European XFEL. A 400 nm optical laser (OL) pulse excites the sample for every other X-ray pulse. (b) Molecular structure of CNCbl where the central corrin ring is highlighted in blue. (c) The CNCbl Jablonski diagram.

The limited use of soft X-ray techniques stems from the strong material absorption in

the soft X-ray regime. X-ray penetration depths for liquid samples are on the order of  $\sim 0.5\text{-}5\ \mu\text{m}$  depending on the solvent and photon energy, and experiments must be carried out in vacuum environments, which complicates sample handling. In the picosecond time regime, transmission mode XAS with soft X-rays is a well-established synchrotron technique,<sup>15</sup> which has enabled numerous photophysical and photochemical investigations<sup>16–25</sup> Synchrotron-based measurements can benefit from a MHz repetition rate source, which provides sufficient count rates to average out fluctuations from liquid jet samples. Moving to femtosecond measurements presents a formidable challenge. One option is the “slicing” technique that has been used to perform femtosecond TRXAS at synchrotrons.<sup>26,27</sup> However, due to the technical challenges and limited brightness of this method, there is only a single example for a transition metal L-edge measurement, which required a 100 mM sample.<sup>27</sup> In the case of XFELs, there are a few examples of Fe L-edge and N K-edge XAS, but samples had concentrations  $\geq 300\ \text{mM}$  in the absorbing atom to compensate for low count rates due to the 120 Hz repetition rate of the facility.<sup>28,29</sup> Here, we report a new implementation of femtosecond TRXAS with soft X-rays for dilute liquid samples at a high-repetition rate XFEL. This approach is based on the recently reported beam splitting off-axis zone plate (BOZ)-XAS setup, which has been used to measure solid-state thin-film samples.<sup>30–32</sup>

The BOZ-XAS experimental setup is shown in Figure 1a. Monochromatic X-ray pulses are delivered to the Spectroscopy and Coherent Scattering (SCS) instrument at the SASE3 branch of European XFEL (EuXFEL).<sup>33,34</sup> These X-ray pulses pass through an elliptical BOZ optical element, which combines a transmission grating and zone plate to both split and focus the beam. The three beams created by the BOZ are detected on a pixel detector, the DSSC,<sup>35</sup> that reads out the signal from each X-ray pulse. The central beam from the BOZ passes through a flat liquid jet giving the transmitted intensity ( $I_t$ ), while the side beams freely propagate providing the reference measurements ( $I_{0a}$  and  $I_{0b}$ ). Due to the MHz read-out rate of the DSSC, the setup is able to take full advantage of the high-repetition rate of EuXFEL depicted in Figure 1a. EuXFEL delivers 10 “pulse trains” per second. In the

results reported here, each train contained 400 x-ray pulses yielding an effective repetition rate of 4 kHz.

In the following we demonstrate this new experimental capability by determining the electronic character of the lowest-lying excited state of cyanocobalamin (CNCbl), a representative cobalamin complex. The cobalamin cofactor is best known for its ground state chemistry,<sup>36</sup> but also acts as photo-switch controlling carotenoid production in bacteria and is actively investigated for potential photochemical applications.<sup>37</sup> Figure 1b shows the structure of CNCbl where the low-spin  $\text{Co}^{3+}$  ( $3d^6$ ) atom is bound by the corrin ring and axial ligands. The excited state dynamics of CNCbl have been previously studied by ultrafast optical and hard X-ray techniques.<sup>5,6,38</sup> Its photophysics can be summarized in the simplified scheme shown in Figure 1c. Light absorption creates a corrin-centered  $\pi \rightarrow \pi^*$  excited state ( $S_n$ ), which undergoes internal conversion to a structurally distorted state,  $S_1$ , within a few hundred fs. The  $S_1$  geometric structure exhibits  $\sim 0.2$  Å elongation of the axial Co-C and Co-N bonds, which indicates the population of the Co  $d_{z^2}$  orbital. Time-dependent density functional theory (TDDFT) calculations have suggested that this state is a corrin  $\pi \rightarrow \text{Co } d_{z^2}$  ligand to metal charge transfer (LMCT) state.<sup>39</sup> However, the Co  $d_{z^2}$  orbital could also be populated via a metal-centered (MC) excitation ( $3d_\pi \rightarrow d_{z^2}$ ). The  $L_3$ -edge TRXAS provides a sensitive observable to characterize the Co 3d orbital occupations and consequently the  $S_1$  state identity. First, we present the TRXAS measurements demonstrating the high-sensitivity of the BOZ-XAS setup. Next, L-edge XAS is compared with ligand field multiplet theory (LMFT) simulations, which indicate that the  $S_1$  state is predominantly a MC rather than LMCT excited state. This conclusion is further supported by new TDDFT calculations performed at the excited state geometry.

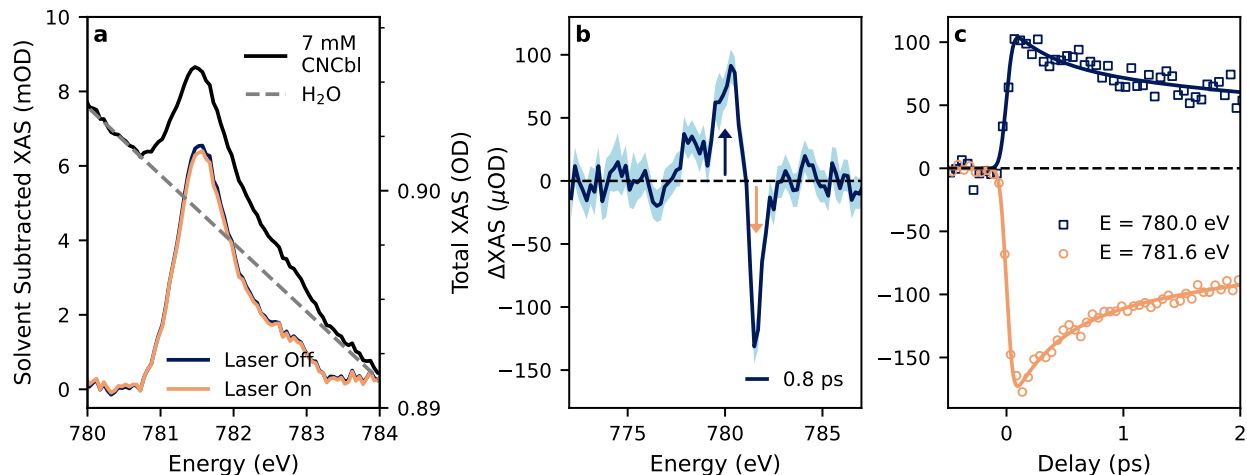


Figure 2:  $L_3$ -edge XAS of Cyanocobalamin. (a) Total absorbance of solvent plus 7 mM cyanocobalamin (right axis). The solvent subtracted spectra are shown for laser off (blue) and laser on (orange) measurements (left axis). (b) TRXAS spectrum measured at a 0.8 ps delay between the 400 nm pump and X-ray probe beam. The shaded region depicts the standard error for each data point, and vertical arrows denote the energies of the delay traces. (c) The time dependence of the transient XAS signal was measured at 780 and 781.6 eV. The solid lines show a simultaneous bi-exponential fit to the data.

## Results and Discussion

Figure 2a shows the total and solvent-subtracted XAS signals for the  $L_3$ -edge of 7 mM cyanocobalamin in water. The total absorbance shown in black has a level of 0.9 OD (right axis) and is almost entirely due to the solvent background (dashed gray line). Using tabulated values of the X-ray absorption cross section of water at 780 eV, this corresponds to a liquid jet thickness of  $\sim 2.7 \mu\text{m}$ .<sup>40</sup> The background-subtracted cobalamin absorption (colored curves) is two orders of magnitude smaller (left axis) with a maximum of 7 mOD at 781.6 eV. It is shown for both laser-on and laser-off shots. The two spectra are nearly indistinguishable on the scale of the background-subtracted solute absorbance. The spectrum contains a single sharp feature with a high-energy shoulder. This is consistent with other low-spin six-coordinate Co(III) complexes.<sup>41,42</sup>

The transient XAS is shown in Figures 2b and c for energy and time scans, respectively. The energy scan collected 0.8 ps after laser excitation exhibits three clear features that rise above the baseline noise. A sharp depletion is observed at the energy of the ground state

resonance, and two excited state absorption features are centered at 778.2 and 780 eV. The maximum amplitudes of the three features are 35, 90, and 130  $\mu\text{OD}$ . The error bars on the spectrum are given by the standard errors of the measurements, and with the 0.2 eV energy step shown here, the mean error is 12  $\mu\text{OD}$ , which is equivalent to a relative transmission change of  $< 4 \times 10^{-5}$ . Delay traces collected at 780.0 and 781.6 eV have been simultaneously fitted with biexponential decays convolved with a Gaussian instrument response function (as described in detail in the SI). The fitted width of the instrument response function yields a time resolution of  $106 \pm 10$  fs FWHM, which validates the  $\sim 100$  fs time resolution of the measurement. The long time constant has been fixed to 7.25 ps to match the value determined by optical transient absorption for the ground state recovery for CNCbl at 8  $^{\circ}\text{C}$ .<sup>43</sup> The 8  $^{\circ}\text{C}$  reference value was used because, although experiments were performed with a room temperature sample reservoir, evaporative cooling from the in-vacuum flat jet is expected to reduce the sample temperature significantly.<sup>44</sup> The fast time constant was found to be 390 fs. This is attributed to the internal conversion from the Franck-Condon region of the initially ligand-centered excited state through any intermediate states to the  $S_1$  state. This relaxation time is somewhat longer than the 190 fs time constant found for excitation at 520 nm.<sup>5,45</sup> This difference may be due to the 400 nm excitation used in the present study, a difference in temperature, or the choice of photon energy for the time traces. Overall, it is consistent with the timescales of internal conversion (0.2 - 0.6 ps) previously reported for cobalamin compounds.<sup>38,43</sup> The transient spectrum measured at 0.8 ps is temporally separated from the excited state cascade and must be due to the  $S_1$  electronic state as identified in previous measurements.

We begin by analyzing the character of the  $S_1$  state by comparing the data with common heuristics for interpreting L-edge XAS. First, it can be seen that the integral of the difference spectrum in Figure 2b is positive. This is the opposite of what would be expected for a corrin  $\pi \rightarrow \text{Co } d_{z^2}$  LMCT state because the integrated L-edge intensity is proportional to the number of vacant 3d orbitals.<sup>46,47</sup> Second, the excited state spectrum may be constructed

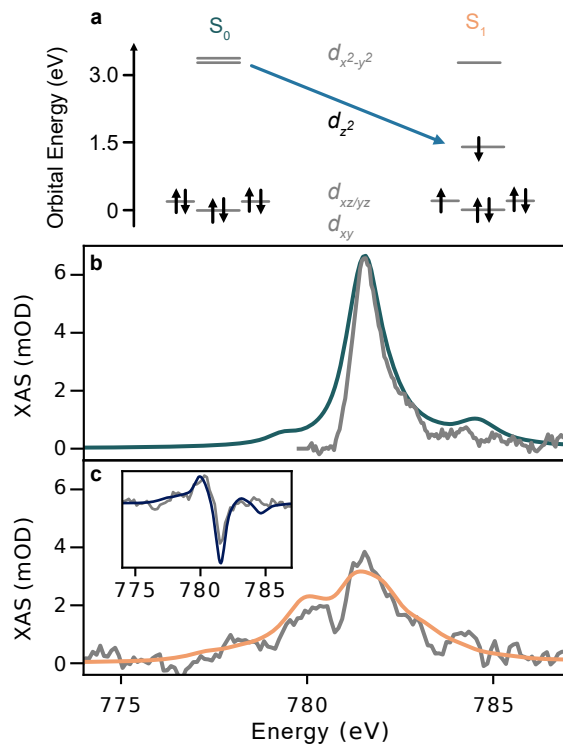


Figure 3: Multiplet simulations of CNCbl XAS. (a) Depicts the energies and occupations of the Co 3d-orbitals in  $S_0$  and  $S_1$  states within the approximation of  $D_{4h}$  symmetry. (b) and (c) show comparisons of the measured XAS spectrum (gray) with ligand field theoretical simulations (blue) for  $S_0$  and  $S_1$  states, respectively. The inset in (c) shows the comparison between the measured and theoretical transient XAS spectrum at 0.8 ps delay.

from the ground state spectrum and the difference spectrum with knowledge of the excited state fraction as described in the SI. It is found that the shift in the  $L_3$ -edge energy is not significant for any reasonable choice of excited state fraction (see Figure S8c and associated discussion). This also suggests an LMCT  $S_1$  state is unlikely because typical L-edge shifts associated with oxidation state changes are  $\sim 0.7$ - $1.5$  eV.<sup>10,12,41,48</sup> Instead, this spectrum is consistent with the formation of a  $d_\pi \rightarrow d_{z^2}$  MC excited state. Such a state has an occupied  $d_{z^2}$  orbital, which is consistent with the axially distorted geometry identified in previous experiments.<sup>5,6</sup> Further, the formation of a hole in the  $3d_\pi$  and changes in the ligand field strength would give rise to the new low-energy features in the difference spectrum at 778.2 and 780 eV.

LFMT simulations within  $D_{4h}$  symmetry are used to assess the possibility of an MC

excited state. The relative orbital energies of the ligand field model for both the  $S_0$  and  $S_1$  states are shown in Figure 3a. The complete set of simulation parameters is given in Table S4. Figure 3b shows the comparison between the simulated and experimental ground state spectrum. The simulation reproduces the single intense absorption feature centered at 781.6 eV. We note that the experimental spectrum is missing intensity in the pre-edge region. This is due to complications with the background subtraction, as discussed in the SI (see S6 and S9). The simulated spectrum of the  $S_1$  state is shown in Figure 3c together with the experimental  $S_1$  state constructed for a 5% excitation fraction. There is good agreement between the simulated and experimental spectrum with the most intense feature remaining at 778.6 eV, but new features appearing between 777.5 and 781 eV. As in the ground state, a lack of absorption around 780 eV persists due to the use of the ground state spectrum in constructing the  $S_1$  spectrum.

Although the L-edge XAS is comprised of transitions between the many electron states, the observed XAS lineshapes can be understood in terms of the orbital picture presented in Figure 3a. The ground state possesses a nearly octahedral ligand field with the  $3d_{\sigma^*}$  and  $3d_{\pi}$  orbitals split by an average of 3.2 eV. Thus, the single intense feature at 781.6 eV is due to  $2p \rightarrow 3d_{\sigma^*}$  transitions. In the geometrically distorted excited state, the  $d_{z^2}$  orbital energy decreases to 1.4 eV above the energy of the  $d_{xy}$  orbital in the LFMT model as depicted by the arrow in Figure 3a. Thus, the new lower energy features at 780 and 778.2 eV are expected to have significant contributions from excitations to the singly occupied orbitals,  $d_{z^2}$  and either  $d_{xz}$  or  $d_{yz}$ . The feature at 781.6 eV is unshifted from the ground state, and because there is not a large change in the in-plane ligand field, this peak is attributed to  $2p \rightarrow 3d_{x^2-y^2}$  transitions. These assignments are confirmed by orbital population difference spectra shown in Figure S11, and the chosen ligand field parameters are in good agreement with those predicted by *ab initio* ligand field theory (see SI for details).

The excited states of cobalamin have previously been investigated by TDDFT with the goal of interpreting optical spectra. Kozłowski and coworkers have argued that the BP86<sup>49,50</sup>

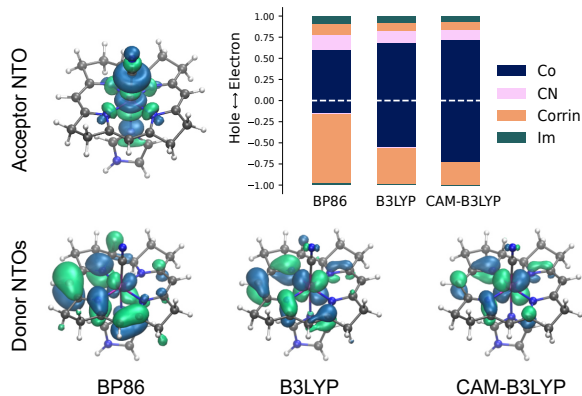


Figure 4: Natural transition orbitals (NTOs) for the  $S_1$  state computed with BP86, B3LYP, and CAM-B3LYP functionals. The acceptor NTO is similar across all functionals (top left), while the donor NTO (bottom) differs across the series. Fragment analysis of electron and hole fractions is given for the Co center and each ligand at the top right.

functional gives the best agreement between theory and experiment by comparison of homogeneously broadened TDDFT transitions and experimental spectra.<sup>51–54</sup> On the other hand, Brunold and coworkers have found B3LYP<sup>55</sup> to be suitable.<sup>56,57</sup> In particular, a recent study suggested that BP86 TDDFT optical spectra suffer from spurious low-energy charge transfer contributions that mimic vibronic structures, and it was concluded that B3LYP provides a better agreement with experiment once the effects of vibrations are included.<sup>57</sup> Most studies have been carried out at the ground state geometry, except for the work of Lodowski *et al.*, which employed the BP86 functional, explored the excited state potential energy surfaces and found that the  $S_1$  state was an LMCT state.<sup>39</sup>

Given the ongoing debate over which DFT approximations are most suitable for describing the excited states of cobalamins, we examined the functional dependence of the excited state character at the geometry of the  $S_1$  state. The calculations were performed on a reduced structural model for CNCbl,  $[\text{ImCo}(\text{corrin})\text{CN}]^+$ , that has commonly been employed in other theoretical studies. Figure 4 shows the character of the  $S_1$  excited state for various levels of DFT theory at the excited state geometry for BP86, B3LYP, and CAM-B3LYP.<sup>58</sup> This is represented by the natural transition orbitals (NTOs), which have, in this case, only a single significant ( $> 97\%$ ) donor–acceptor orbital pair for the lowest-lying singlet transition.

The transitions are further quantified by fragment analysis of electron and hole fractions on the metal and each of the ligands.<sup>59</sup> Regardless of the functional chosen, the excitation is a mixture of LMCT and MC, with both ligand and metal character for both the donor and acceptor orbitals. The character of the acceptor orbital is independent of functional, which is Co  $d_{z^2}$  with a significant  $\text{CN}^-$  lone pair contribution. The hole NTO is a mixture of corrin  $\pi$  and  $d_{xz/yz}$  character. Co exhibits a strong functional dependence that changes the excitation from primarily LMCT for BP86 to MC for the range-separated hybrid CAM-B3LYP. The  $L_3$ -edge XAS is more consistent with the results from the hybrid functionals (B3LYP and CAM-B3LYP), which show a significant MC excited state fraction and are generally expected to provide a more accurate treatment of charge transfer excitations. The hybrid functional results are qualitatively consistent with the multiplet simulations as they exhibit  $d_{xz/yz}$  hole character and a singly occupied  $d_{z^2}$  orbital. Thus, we conclude that the  $S_1$  state of cobalamin is primarily a MC excited state but still likely possesses some fractional charge transfer from the corrin ring. We note, however, that there is only a moderate change in the charge density on the Co for these cases because charge transfer from the corrin ring is partially delocalized onto the  $\text{CN}^-$  ligand rather than increasing the electron density on the Co atom. This is consistent with the interpretation of the spectrum from the multiplet simulations where no shift in the  $2p \rightarrow d_{x^2-y^2}$  feature is observed. A more precise quantification of the CT would require a more sophisticated theoretical model for computing the XAS spectra. This could take the form of a model Hamiltonian that includes differential  $\pi$  and  $\sigma$ -CT, or alternatively, an *ab initio* approach based on multiconfigurational wavefunctions. Such investigations are left to future studies.

## Conclusions

Here we have used TRXAS at the L-edge of Co to identify MC character in the CNCbl  $S_1$  state. These results demonstrate how the state selectivity of L-edge XAS can be used

to elucidate photophysical mechanisms in coordination complexes. We emphasize that this study has only been made possible because of the implementation of the BOZ-XAS approach at a high repetition-rate XFEL. The  $\sim 10$  mM solubility limit, ultrafast excited state cascade, and the 7 ps ground state recovery timescale necessitated a high signal-to-noise ratio and femtosecond time resolution.

The capability presented in this work greatly changes the scope of chemical problems that can be addressed by soft X-ray spectroscopy for liquid samples. For the time-resolved data presented in Figure 2, each energy and delay scan represents 40 minutes of measurement or  $\sim 2$  hours of total experimental time. These data provide an indication of expected data collection times for more dilute samples, and samples with a concentration of 1.75 mM and similar excitation fraction could be investigated with similar S/N within 32 hours of measurement time. This measurement time is accessible with standard beamtime allocations enabling time-resolved soft X-ray studies on many synthetic coordination complexes and some important metallo-enzymes. For example, heme enzymes such as cytochrome c and myoglobin have been studied with ultrafast hard X-ray spectroscopy at concentrations of 3-4 mM.<sup>3,8</sup> With the continued development of XFELs targeting full MHz operation, the measurement scheme presented here could gain two additional orders of magnitude in data collection speed, paving the way to measuring systems at the  $100\mu\text{M}$  concentration.

## Supporting Information Available

Details of the experimental setup and measurement parameters. Description of data processing and analysis. Theoretical and computational methods with additional analysis.

## Acknowledgement

We acknowledge European XFEL in Schenefeld, Germany, for the provision of X-ray free-electron laser beamtime at the SCS Instrument under proposal number UP3423 and would

like to thank the staff for their assistance. Data recorded for the experiment at the European XFEL are available at doi:10.22003/XFEL.EU-DATA-003423-00. The powder XAS spectrum was measured at the BOREAS beamline at ALBA Synchrotron in collaboration with ALBA staff as part of Proposal 2023097863. This research was supported in part through the Maxwell computational resources operated at Deutsches Elektronen-Synchrotron DESY, Hamburg, Germany. N. G., A. S., and B. V. K. acknowledge the European XFEL R&D program for financial support. This work was supported in part by a grant from the National Science Foundation NSF-CHE 2154157 to RJS M.H. acknowledges funding by the German Federal Ministry of Education and Research under grant number 13K22XXB DY- leLUXIT. Z.Y. was supported by the JSPS KAKENHI program Grant No. 25H00864.

## References

- (1) Chen, L. X.; Zhang, X.; Shelby, M. L. Recent advances on ultrafast X-ray spectroscopy in the chemical sciences. *Chem. Sci.* **2014**, *5*, 4136–4152.
- (2) Chergui, M.; Collet, E. Photoinduced Structural Dynamics of Molecular Systems Mapped by Time-Resolved X-ray Methods. *Chem. Rev.* **2017**, *117*, 11025–11065.
- (3) Mara, M. W. et al. Metalloprotein entatic control of ligand-metal bonds quantified by ultrafast x-ray spectroscopy. *Science* **2017**, *356*, 1276–1280.
- (4) Shelby, M. L.; Lestrangle, P. J.; Jackson, N. E.; Haldrup, K.; Mara, M. W.; Stickrath, A. B.; Zhu, D.; Lemke, H. T.; Chollet, M.; Hoffman, B. M.; Li, X.; Chen, L. X. Ultrafast Excited State Relaxation of a Metalloporphyrin Revealed by Femtosecond X-ray Absorption Spectroscopy. *J. Am. Chem. Soc.* **2016**, *138*, 8752–8764.
- (5) Miller, N. A.; Deb, A.; Alonso-Mori, R.; Garabato, B. D.; Glowina, J. M.; Kiefer, L. M.; Koralek, J.; Sikorski, M.; Spears, K. G.; Wiley, T. E.; Zhu, D.; Kozlowski, P. M.; Kubarych, K. J.; Penner-Hahn, J. E.; Sension, R. J. Polarized XANES monitors fem-

- tosecond structural evolution of photoexcited Vitamin B12. *J. Am. Chem. Soc.* **2017**, *139*, 1894–1899.
- (6) Miller, N. A. et al. Ultrafast X-ray Absorption Near Edge Structure Reveals Ballistic Excited State Structural Dynamics. *J. Phys. Chem. A.* **2018**, *122*, 4963–4971.
- (7) Miller, N. A.; Michocki, L. B.; Konar, A.; Alonso-Mori, R.; Deb, A.; Glownia, J. M.; Sofferman, D. L.; Song, S.; Kozlowski, P. M.; Kubarych, K. J.; Penner-Hahn, J. E.; Sension, R. J. Ultrafast XANES Monitors Femtosecond Sequential Structural Evolution in Photoexcited Coenzyme B12. *J. Phys. Chem. B.* **2020**, *124*, 199–209.
- (8) Bacellar, C. et al. Doming and spin cascade in Ferric Haems: Femtosecond X-ray Absorption and X-ray Emission Studies. *Proc. Natl. Acad. Sci. U.S.A.* **2020**, *117*, 21914–21920.
- (9) Shelby, M. L.; Wildman, A.; Hayes, D.; Mara, M. W.; Lestrangle, P. J.; Cammarata, M.; Balducci, L.; Artamonov, M.; Lemke, H. T.; Zhu, D.; Seideman, T.; Hoffman, B. M.; Li, X.; Chen, L. X. Interplays of electron and nuclear motions along co dissociation trajectory in myoglobin revealed by ultrafast x-rays and quantum dynamics calculations. *Proc. Natl. Acad. Sci. U.S.A.* **2021**, *118*, 1–11.
- (10) Cramer, S. P.; DeGroot, F. M. F.; Ma, Y.; Chen, C. T.; Sette, F.; Kipke, C. A.; Eichhorn, D. M.; Chan, M. K.; Armstrong, W. H.; Libby, E.; Christou, G.; Brooker, S.; McKee, V.; Mullins, O. C.; Fuggle, J. C. Ligand field strengths and oxidation states from manganese L-edge spectroscopy. *J. Am. Chem. Soc.* **1991**, *113*, 7937–7940.
- (11) de Groot, F. M. F. Multiplet effects in X-ray spectroscopy. *Coord. Chem. Rev.* **2005**, *249*, 31–63.
- (12) Hocking, R. K.; Wasinger, E. C.; de Groot, F. M. F.; Hodgson, K. O.; Hedman, B.; Solomon, E. I. Fe L-edge XAS studies of K<sub>4</sub>[Fe(CN)<sub>6</sub>] and K<sub>3</sub>[Fe(CN)<sub>6</sub>]: a direct probe of back-bonding. *J. Am. Chem. Soc.* **2006**, *128*, 10442–51.

- (13) Hocking, R. K.; Wasinger, E. C.; Yan, Y.-L.; Degroot, F. M. F.; Walker, F. A.; Hodgson, K. O.; Hedman, B.; Solomon, E. I. Fe L-edge X-ray absorption spectroscopy of low-spin heme relative to non-heme Fe complexes: delocalization of Fe d-electrons into the porphyrin ligand. *J. Am. Chem. Soc.* **2007**, *129*, 113–25.
- (14) Glaser, T.; Hedman, B.; Hodgson, K. O.; Solomon, E. I. Ligand K-Edge X-ray Absorption Spectroscopy: A Direct Probe of Ligand–Metal Covalency. *Acc. Chem. Res.* **2000**, *33*, 859–868.
- (15) Fondell, M. et al. Time-resolved soft X-ray absorption spectroscopy in transmission mode on liquids at MHz repetition rates Time-resolved soft X-ray absorption spectroscopy in transmission mode on liquids at MHz repetition rates. *Struct. Dyn.* **2017**, *4*, 054902.
- (16) Huse, N.; Kim, T. K.; Jamula, L.; McCusker, J. K.; de Groot, F. M. F.; Schoenlein, R. W. Photo-Induced Spin-State Conversion in Solvated Transition Metal Complexes Probed via Time-Resolved Soft X-ray Spectroscopy. *J. Am. Chem. Soc.* **2010**, *132*, 6809–6816.
- (17) Cho, H.; Strader, M. L.; Hong, K.; Jamula, L.; Gullikson, E. M.; Kim, T. K.; De Groot, F. M. F.; McCusker, J. K.; Schoenlein, R. W.; Huse, N. Ligand-field symmetry effects in Fe(ii) polypyridyl compounds probed by transient X-ray absorption spectroscopy. *Faraday Discuss.* **2012**, *157*, 463.
- (18) Van Kuiken, B.; Cho, H.; Hong, K.; Khalil, M.; Schoenlein, R.; Kim, T. K.; Huse, N. Time-Resolved X-ray Spectroscopy in the Water Window: Elucidating Transient Valence Charge Distributions in an Aqueous Fe(II) Complex. *J. Phys. Chem. Lett.* **2016**, *7*, 465 – 470.
- (19) Cordones, A. A.; Pemmaraju, C. D.; Lee, J. H.; Zegkinoglou, I.; Ragoussi, M.-E.; Himpsel, F. J.; de la Torre, G.; Schoenlein, R. W. Excited-State Charge Distribution

- of Donor-pi-Acceptor Zn Porphyrin Probed by N K-edge Transient Absorption Spectroscopy. *J. Phys. Chem. Lett.* **2021**, *12*, 1182–1188.
- (20) Cruz, V. V. d.; J. Mascarenhas, E.; Büchner, R.; M. Jay, R.; Fondell, M.; Eckert, S.; Föhlisch, A. Metal–water covalency in the photo-aquated ferrocyanide complex as seen by multi-edge picosecond X-ray absorption. *Phys. Chem. Chem. Phys.* **2022**, *24*, 27819–27826.
- (21) Mascarenhas, E. J.; Fondell, M.; Büchner, R.; Eckert, S.; Vaz Da Cruz, V.; Föhlisch, A. The Role of the Lowest Excited Triplet State in Defining the Rate of Photoaquation of Hexacyanometalates. *J. Phys. Chem. Lett.* **2024**, 241–247.
- (22) Wallick, R. F.; Chakrabarti, S.; Burke, J. H.; Gnewkow, R.; Chae, J. B.; Rossi, T. C.; Mantouvalou, I.; Kanngießer, B.; Fondell, M.; Eckert, S.; Dykstra, C.; Smith, L. E.; Vura-Weis, J.; Mirica, L. M.; Van Der Veen, R. M. Excited-State Identification of a Nickel-Bipyridine Photocatalyst by Time-Resolved X-ray Absorption Spectroscopy. *J. Phys. Chem. Lett.* **2024**, *15*, 4976–4982.
- (23) Jay, R. M.; Coates, M. R.; Zhao, H.; Winghart, M.-O.; Han, P.; Wang, R.-P.; Harich, J.; Banerjee, A.; Wikmark, H.; Fondell, M.; Nibbering, E. T. J.; Odelius, M.; Huse, N.; Wernet, P. Photochemical Formation and Electronic Structure of an Alkane  $\sigma$ -Complex from Time-Resolved Optical and X-ray Absorption Spectroscopy. *J. Am. Chem. Soc.* **2024**, *146*, 14000–14011.
- (24) Ghodrati, N.; Eckert, S.; Fondell, M.; Scherz, A.; Föhlisch, A.; Van Kuiken, B. E. Identification of metal-centered excited states in Cr(III) complexes with time-resolved L-edge X-ray spectroscopy. *Chem. Sci.* **2025**, 6307–6316.
- (25) Burke, J. H. et al. How Does Metal Spin State Affect Electronic Communication in Mixed-Valence Dimers? Insights from Ultrafast Near-Infrared and Soft X-ray Transient Absorption Spectroscopy. *Inorg. Chem.* **2026**,

- (26) Wen, H.; Huse, N.; Schoenlein, R. W.; Lindenberg, A. M. Ultrafast conversions between hydrogen bonded structures in liquid water observed by femtosecond x-ray spectroscopy. *J. Chem. Phys.* **2009**, *131*, 234505.
- (27) Huse, N.; Cho, H.; Hong, K.; Jamula, L.; de Groot, F. M. F.; Kim, T. K.; McCusker, J. K.; Schoenlein, R. W. Femtosecond Soft X-ray Spectroscopy of Solvated Transition-Metal Complexes: Deciphering the Interplay of Electronic and Structural Dynamics. *J. Phys. Chem. Lett.* **2011**, *2*, 880–884.
- (28) Jay, R. M. et al. Disentangling Transient Charge Density and Metal–Ligand Covalency in Photoexcited Ferricyanide with Femtosecond Resonant Inelastic Soft X-ray Scattering. *J. Phys. Chem. Lett.* **2018**, *9*, 3538–3543.
- (29) Jay, R. M. et al. Following Metal-to-Ligand Charge-Transfer Dynamics with Ligand and Spin Specificity Using Femtosecond Resonant Inelastic X-ray Scattering at the Nitrogen K-Edge. *J. Phys. Chem. Lett.* **2021**, *12*, 6676–6683.
- (30) Le Guyader, L. et al. Photon-shot-noise-limited transient absorption soft X-ray spectroscopy at the European XFEL. *J. Synchrotron Rad.* **2023**, *30*, 284–300.
- (31) Lojewski, T. et al. The interplay of local electron correlations and ultrafast spin dynamics in fcc Ni. *Mater. Res. Lett.* **2023**, *11*, 655–661.
- (32) Kämmerer, L. et al. Femtosecond Spin-State Switching Dynamics of Fe(II) Complexes Condensed in Thin Films. *ACS Nano* **2024**, *18*, 34596–34605.
- (33) Carley, R.; van Kuiken, B.; Le Guyader, L.; Mercurio, G.; Scherz, A. *SCS Instrument Review Report*; XFEL.EU TR-2022-003, European XFEL GmbH: Schenefeld, Germany, 2022, <http://doi.org/10.22003/XFEL.EU-TR-2022-003>.
- (34) Decking, W. et al. A MHz-repetition-rate hard X-ray free-electron laser driven by a superconducting linear accelerator. *Nature Photonics* **2020**, *14*, 391–397.

- (35) Porro, M. et al. The MiniSDD-Based 1-Mpixel Camera of the DSSC Project for the European XFEL. *IEEE Trans. Nucl. Sci.* **2021**, *68*, 1334–1350.
- (36) Banerjee, R.; Ragsdale, S. W. The Many Faces of Vitamin B<sub>12</sub> : Catalysis by Cobalamin-Dependent Enzymes. *Annu. Rev. Biochem.* **2003**, *72*, 209–247.
- (37) Jones, A. R. The photochemistry and photobiology of vitamin B12. *Photochem. Photobiol. Sci.* **2017**, *16*, 820–834.
- (38) Rury, A. S.; Wiley, T. E.; Sension, R. J. Energy Cascades, Excited State Dynamics, and Photochemistry in Cob(III)alamins and Ferric Porphyrins. *Acc. Chem. Res.* **2015**, *48*, 860–867.
- (39) Lodowski, P.; Jaworska, M.; Andruniów, T.; Garabato, B. D.; Kozłowski, P. M. Mechanism of the S1 excited state internal conversion in vitamin B12. *Phys. Chem. Chem. Phys.* **2014**, *16*, 18675–18679.
- (40) Henke, B. L.; Gullikson, E. M.; Davis, J. C. X-Ray Interactions: Photoabsorption, Scattering, Transmission, and Reflection at  $E = 50\text{--}30,000$  eV,  $Z = 1\text{--}92$ . *At. Data Nucl. Data Tables* **1993**, *54*, 181–342.
- (41) Sreekantan Nair Lalithambika, S.; Golnak, R.; Winter, B.; Atak, K. Electronic Structure of Aqueous [Co(bpy)<sub>3</sub>]<sup>2+/3+</sup> Electron Mediators. *Inorg. Chem.* **2019**, *58*, 4731–4740.
- (42) Guo, M.; Liu, X.; He, R. Restricted active space simulations of the metal L-edge X-ray absorption spectra and resonant inelastic X-ray scattering: revisiting [CoII/III(bpy)<sub>3</sub>]<sup>2+/3+</sup>. *Inorg. Chem. Front.* **2020**, *7*, 1927–1938.
- (43) Harris, D. A.; Stickrath, A. B.; Carroll, E. C.; Sension, R. J. Influence of Environment on the Electronic Structure of Cob(III)alamins: Time-Resolved Absorption Studies of the S1 State Spectrum and Dynamics. *J. Am. Chem. Soc.* **2007**, *129*, 7578–7585.

- (44) Chang, Y.-P.; Yin, Z.; Balciunas, T.; Wörner, H. J.; Wolf, J.-P. Temperature measurements of liquid flat jets in vacuum. *Struct. Dyn.* **2022**, *9*, 014901.
- (45) Shiang, J. J.; Cole, A. G.; Sension, R. J.; Hang, K.; Weng, Y.; Trommel, J. S.; Marzilli, L. G.; Lian, T. Ultrafast Excited-State Dynamics in Vitamin B<sub>12</sub> and Related Cob(III)alamins. *J. Am. Chem. Soc.* **2006**, *128*, 801–808.
- (46) Wang, H.; Ge, P.; Riordan, C. G.; Brooker, S.; Woome, C. G.; Collins, T.; Melendres, C. A.; Graudejus, O.; Bartlett, N.; Cramer, S. P. Integrated X-ray L Absorption Spectra. Counting Holes in Ni Complexes. *J. Phys. Chem. B.* **1998**, *102*, 8343–8346.
- (47) Wang, H.; Friedrich, S.; Li, L.; Mao, Z.; Ge, P.; Balasubramanian, M.; Patil, D. S. L-edge sum rule analysis on 3d transition metal sites: from d<sup>10</sup> to d<sup>0</sup> and towards application to extremely dilute metallo-enzymes. *Phys. Chem. Chem. Phys.* **2018**, *20*, 8166–8176.
- (48) Tan, H.; Verbeeck, J.; Abakumov, A.; Van Tendeloo, G. Oxidation state and chemical shift investigation in transition metal oxides by EELS. *Ultramicroscopy* **2012**, *116*, 24–33.
- (49) Becke, A. D. Density-functional exchange-energy approximation with correct asymptotic behavior. *Phys. Rev. A* **1988**, *38*, 3098–3100.
- (50) Perdew, J. Density-functional approximation for the correlation energy of the inhomogeneous electron gas. *Phys. Rev. B* **1986**, *33*, 8822–8824.
- (51) Andruniów, T.; Kozłowski, P. M.; Zgierski, M. Z. Theoretical analysis of electronic absorption spectra of vitamin B<sub>12</sub> models. *J. Chem. Phys.* **2001**, *115*, 7522–7533.
- (52) Kornobis, K.; Kumar, N.; Wong, B. M.; Lodowski, P.; Jaworska, M.; Andruniów, T.; Ruud, K.; Kozłowski, P. M. Electronically excited states of vitamin B<sub>12</sub>: Benchmark

- calculations including time-dependent density functional theory and correlated ab initio methods. *J. Phys. Chem. A* **2011**, *115*, 1280–1292.
- (53) Solheim, H.; Kornobis, K.; Ruud, K.; Kozłowski, P. M. Electronically Excited States of Vitamin B12 and Methylcobalamin: Theoretical Analysis of Absorption, CD, and MCD Data. *J. Phys. Chem. B* **2011**, *115*, 737–748.
- (54) Lodowski, P.; Jaworska, M.; Kornobis, K.; Andruniów, T.; Kozłowski, P. M. Electronic and structural properties of low-lying excited states of vitamin B12. *Journal of Physical Chemistry B* **2011**, *115*, 13304–13319.
- (55) Becke, A. D. A new mixing of Hartree–Fock and local density-functional theories. *J. Chem. Phys.* **1993**,
- (56) Stich, T. A.; Brooks, A. J.; Buan, N. R.; Brunold, T. C. Spectroscopic and Computational Studies of Co<sup>3+</sup>-Corrinoids: Spectral and Electronic Properties of the B<sub>12</sub> Cofactors and Biologically Relevant Precursors. *J. Am. Chem. Soc.* **2003**, *125*, 5897–5914.
- (57) Elmendorf, L. D.; Brunold, T. C. Vibronic Coupling in Vitamin B<sub>12</sub> : A Combined Spectroscopic and Computational Study. *Inorg. Chem.* **2023**, *62*, 12762–12772.
- (58) Yanai, T.; Tew, D.; Handy, N. A new hybrid exchange–correlation functional using the Coulomb-attenuating method (CAM-B3LYP). *Chem. Phys. Lett.* **2004**, *393*, 51–57.
- (59) Plasser, F. TheoDORE: A toolbox for a detailed and automated analysis of electronic excited state computations. *J. Chem. Phys.* **2020**, *152*, 084108.